Understanding the energy transfer mechanism in the near field of impact driven piles

Athina Grizi[1], Adda Athanasopoulos-Zekkos[2], and Richard D. Woods[2]

ABSTRACT

Pile installation by applying an impact to the top of a pile appears to be a simple construction process but analysis of that process is complicated as it involves a source of energy, the structural member (pile), and the ground into which the pile is driven. Codes and regulatory standards suggest some basic guidance to analysis but much is still unknown. Pile driving creates vibrations in the surrounding ground that can cause direct damage to nearby structures, cracking in underground utilities or dynamic settlement of loose sands with attendant potential damage. It is customary to monitor surface ground motions starting as close as 1.5 m from the pile and use the surface vibration data to interpret energy propagation. The work described here, however, presents ground motion measurements from impact pile driving not only along the surface but also in the body of the ground at different radial distances and depths. Ground motion data during impact pile driving was obtained by installing motion sensors starting very close to the pile, 0.2 m, and moving away to about 0.8 m and 2 m at the same depth as well as along the ground surface at greater distances. Extensive analysis of the ground motion amplitude and dominant frequencies was performed. Shear wave velocity degradation in the near field of an impact driven pile was

[1] University of Nottingham, Department of Civil Engineering, B55 Coates Building, University Park, Nottingham, NG7 2RD, United Kingdom (corresponding author) E-mail: a.gkrizi@nottingham.ac.uk
[2] University of Michigan, Department of Civil and Environmental Engineering, 2350 Hayward St., Ann Arbor, Michigan, 48109, United States of America

evaluated by studying ground motion signatures from the sensor arrays. From the measured ground motion, the hypothesis of three different soil behavior zones (plastic, non-linear and near-linear) surrounding a driven pile was generally confirmed. Also, high frequency vibration near the pile was observed to modify to lower frequencies at greater distance from the pile. All measurements were made at sites where production piles were being driven so coordination with the pile driving contractors was an additional challenge.

Keywords

Pile driving, Impact, H-Piles, Ground vibrations, Shear wave velocity

Introduction

Earth borne vibrations, can cause under some conditions, architectural and/or structural damage to buildings and buried infrastructure. Direct structural damage is not the only consequence from vibration operations though. A combination of loose granular soils and ground vibrations can be the cause of liquefaction, densification and ground settlement, and consequently damage nearby buildings. Problems from pile driving vibrations depend on the dynamic source and the soil medium through which waves will propagate. Various vibration limiting criteria proposed by researchers, governmental agencies and independent standards agencies are usually followed. However, the mechanism of energy transfer from driven piles is complex since the pile is a linear source which is constantly lengthening as it is driven deeper into a soil profile. Therefore, there is a need for understanding the coupling and transmission of the energy into the ground during impact pile driving.

It is imperative to collect ground motion data during full-scale pile driving to obtain a realistic understanding of this complex problem. Common practice is to measure vibration intensities during pile driving operations on the ground surface only, starting at around 2 m from the pile. Placing a geophone closer prevents good coupling of the sensor to the ground because high amplitude ground motions occur in the vicinity of the pile. There are a number of studies [1-11] where surface ground motion measurements have been collected in an attempt to understand how the waves propagate through the ground during pile driving. The work described here represents, for the first time, data collected in close proximity to and in depth from H-piles driven with diesel hammers and the interpretation of that data in terms of energy transfer from pile to ground. Analysis of the ground motion amplitudes, frequency content and shear wave velocity degradation are discussed.

SITE AND INSTRUMENTATION

Site Description

Ground motions during pile driving were monitored by the authors at 5 different project sites controlled by the Michigan Department of Transportation (MDOT) in the State of Michigan. In this paper, results from one site at highway M-139 over Dowagiac River are presented. The M-139 site was associated with the replacement of a deteriorating river bridge near the city of Niles in Michigan. A 16.8 m long 360 mm by 109 kg/m (14 in. by 73 lb/ft) H-pile was driven using a Pileco D30-32 diesel hammer. The final depth of penetration of the pile was 16.2 m. Soil conditions were characterized by standard penetration tests (SPT) and by a combination of the multichannel analysis of surface waves (MASW) technique [12] and the microtremor array measurement (MAM) survey [13]. The soil profile can be generalized as 1.8 m of loose to medium

dense sand (SP) followed by 1.2 m of muck with silt (ML). Below the muck was 1.5 m of loose to medium dense sand (SP) followed by 1.8 m of medium dense silt (ML). Underlying the silt was 2.1 m of loose to medium dense sand (SP) followed by 3 m of medium dense sand (SP). Below the medium dense sand was 4.6 m of dense sand (SP) followed by 2.1 m of very dense sand (SP). Beyond the very dense sand was 3.3 m of dense silt (ML). The water table was encountered at 1.6 m below the ground surface. Figures 1a to 1c show the soil conditions, SPT and Vs profiles and pile penetration resistance, respectively.

Monitoring Procedure

Three triaxial MEMS type accelerometers (Freescale, model MMA7361LC) were pushed to a depth of 7.8 m into a loose to medium dense sand deposit at three different distances from the pile, as shown in Fig. 2. Sacrificial sensor packages were fabricated so that the accelerometer units would be pushed into the ground and be left in place. Standard AW rods were used to push the sensor packages using a drill rig as reaction. Geophones (Mark Products, model L4) were also placed on the ground surface at the locations shown in Fig. 2. Output from all sensors was recorded by a multichannel data acquisition system (National Instruments, model CDAQ-9178) and data logs were taken simultaneously for the whole duration of pile driving and stored in a toughbook computer. A sampling rate of 1 kHz was implemented during data collection. More details about the selection of sensors, installation procedure and data processing can be found in [14-16].

PILE DRIVING VIBRATION MEASUREMENTS

Ground Motions

Three embedded accelerometers were pushed to a depth of 7.8 m at distances of 0.2 m, 0.8 m and 2 m from the driven pile (Fig. 2). The blow with the highest acceleration amplitude per 0.3 m (1 ft) increment of penetration depth was extracted. Figures 3a to 3c present maximum acceleration amplitudes versus depth of the pile tip for the three measured directions, i.e. vertical, longitudinal and transverse. The horizontal black line indicates the common depth of the sensors, while the longitudinal response of accelerometer A4 is not plotted because the signal contained too much noise. The highest ground motion amplitudes are observed for the vertical component of the recorded values. It can be seen in Fig. 3a that the amplitudes increase smoothly as the pile tip approaches the depth of the embedded three-sensor array (7.8 m), with the trend being more evident for the sensor closest to the pile (A3). The increase in vertical and transverse acceleration amplitudes around 11 m may be attributed to the step change in SPT blow counts and the higher penetration resistance as shown in Fig. 1b and 1c, respectively. The spike in amplitude when the pile tip reaches the sensor depth is currently unexplained, but it occurs only for the nearest sensor to the pile (A3) for all three directions. There may be some localized mechanical Poisson's effect of the steel pile on energy wave reflection precisely at the pile tip and that disturbance dissipates rapidly with distance. After the pile tip passes the depth of the sensors, the amplitude of motion remains about constant until diminishing near the end of driving; the pattern is more pronounced for the vertical ground motions.

Figures 4a to 4c present the same vertical acceleration data as shown in Fig. 3a, plotted in terms of the diagonal distance from the pile tip to the buried sensor. The blue solid symbols represent ground motions when the pile tip was still above the elevation of the sensor, while the red open symbols represent data collected when the tip passed below the elevation of the sensor

(7.8 m). For example, by looking at the bottom right square blue symbols and then following them upward to the left in Fig. 4a, we can observe that the amplitude of vibration increases as the pile tip comes closer to the sensor elevation. The diagonal distance is shortest and equal to the horizontal distance from the sensor to the pile (0.2 m) when the tip is at the depth of accelerometer A3. When the tip passes below the sensor, now following the red triangle symbols to the right, the vibration amplitudes decrease at first, then increase and finally decrease close to the end of driving. This behavior can be attributed to spherical body waves expanding by the pile tip and causing all the vibrations at the sensor, while the tip is still above the sensor elevation. When the pile tip goes below the accelerometer, vibrations from the shaft begin to impact the sensor emanating as cylindrical waves. At the same time, the accelerometer can still feel the spherical waves from the tip but as the tip moves deeper and deeper from the sensor, these body waves diminish. These vibration patterns reinforce the hypothesis that spherical waves from the tip dominate the wave field when the pile tip is still above a point in the ground and the cylindrical wave front from the pile shaft starts to contribute when the pile tip goes below that same point in the field [17]. These trends were not proven until now with physical ground motion measurements made very near the driven pile. The same behavior as shown for the vertical component of motion (Fig. 4) was found for the longitudinal and transverse motions.

The conventional method of monitoring ground motions on the ground surface was also followed at this site. The configuration of the surface sensors is shown in Fig. 2. Two triaxial seismometers, BG1 and BG2, were placed on the ground surface at 2 m and 5 m from the pile, respectively. G1 and G2 were single component seismometers measuring vertical and longitudinal motion directions, located at 10.5 m and 12.3 m away from the pile, respectively. Vertical peak

particle velocity versus pile tip depth is presented in Fig. 5a for all the surface sensors. Ground motion records from the surface geophones follow a similar vibration pattern as the buried sensors, i.e. the farther the sensor from the pile the lower the peak particle velocity. There is a decrease in velocity amplitudes when the pile tip is at about 5 m and an increase in amplitudes at about 6.5 m as the pile penetrates into the medium dense silt layer and the penetration resistance increases (Fig. 1). Figures 5b and 5c present the peak particle velocities for the longitudinal and transverse directions of the surface sensors. It is of great interest to notice that the vertical components of motion are smaller than the longitudinal components of motion. This is an indication that the wave motion at these sensors is not a classical Rayleigh wave form as traditionally interpreted by researchers who collect surface ground motion data during pile driving operations [10, 11].

Time histories and Frequency content

Analysis of the individual blows obtained during pile driving was performed in order to study differences in the recorded vibrations in terms of the sensor location and the three components of the sensors. The recorded acceleration pulses were observed to vary with depth and with distance from pile driving. Figures 6 to 8 show vertical, longitudinal and transverse acceleration histories for a single pile driving blow in the time and frequency domain, collected from the buried sensors when the pile tip was at a depth of about 6.5 m; still above the depth of the sensors. The longitudinal record of sensor A4 is not presented because the signal was unstable. The recorded data show that the generated pulses of acceleration lasted approximately 0.2 sec, while the frequency content is distributed over a band lying between 0 and 100 Hz. The peak at about 212.4 sec should be attributed to the ram rebound after the impact with the pile. Obviously, the Fourier spectra are quite different for the three directions (Figs. 6 to 8). For the vertical

direction, which had greater vibration amplitudes than the longitudinal and transverse directions, the dominant vibration frequency was found to be in the range of about 12 to 45 Hz, after studying spectra from impacts at different blow counts during the whole duration of pile driving. For the two horizontal directions however, the records showed that the frequency spectra was in a broader range with dominant frequency peaks reaching about 85 Hz.

Figures 9 to 11 present vertical, longitudinal and transverse acceleration histories for a single pile driving blow in the time and frequency domain, collected from the buried sensors when the pile tip was at a depth of about 9 m; the tip has passed the elevation of the sensors. It is of interest to note that for the vertical vibration records (Fig. 9) the amplitudes of the spectra are larger the closer we are to the pile, i.e. sensor A3 which is closer to the pile recorded larger frequencies distributed in a wider range than the sensors farther away from the pile (A4 and A5). This is not surprising, since waves attenuate with distance and the high frequency content diminishes as the waves propagate farther in the soil mass, moving away from the source. However, this trend is not observed for the two horizontal directions where the dominant frequencies continue to cover a wider range even when the distance from the pile increased.

Shear wave velocity degradation in the near field of a driven pile

As discussed earlier, the MASW and MAM tests were performed to obtain the small strain shear wave velocity profile (Fig. 1b) for the soil zone that the pile was to be driven into. This shear wave velocity profile measured in the far field is significantly higher than in the vicinity of the pile where the soil is under large strains. The decrease of the shear wave velocity can be expressed by Eq 1:

$$V_S = R_S V_{Smax} \quad (1)$$

where:

V_S = shear wave velocity at a given strain, m/sec or ft/sec,

R_S = reduction factor of shear wave velocity, dimensionless, and

V_{Smax} = shear wave velocity at low strain, m/sec or ft/sec.

It is assumed that three different soil behavior zones can be identified around a vibration source [18]:

1. *Plastic zone*: the soil is in failure condition and experiences large shear strain levels of $\gamma > 10^{-1}$ %
2. *Non-linear zone*: some permanent deformations occur and the shear strain levels are between 10^{-3} % < γ < 10^{-1} %
3. *Nearly elastic zone*: no permanent deformations are expected; shear strain levels are below $\gamma < 10^{-3}$ %

The three zones are presented schematically in the vicinity of a driven pile in Fig. 12. As seen in the upper part of Fig. 12, the shear wave velocity is strain dependent and increases with increasing distance from the source. The opposite occurs for the particle velocity; the vibration amplitude attenuates as the waves propagate through the ground and away from the source.

Having installed embedded sensors very close to the pile and then at different radial distances it was possible to calculate the shear wave velocity in the near field zones by inspecting the signals collected by the three accelerometers; A3, A4 and A5. Since the sensors were installed at the same elevation (7.8 m), selection of shear wave arrivals was possible by studying acceleration histories recorded when the pile tip was near the sensors' depth. Shear wave velocities were calculated for three pairs of sensors, i.e. A3 to A4, A4 to A5 and A3 to A5 (Fig. 13). For

example, evaluation of the shear wave arrival time between the two closest accelerometers to the pile, A3 and A4, resulted in a reduction factor of R_S=0.4 for the shear wave velocity. In the same way, analysis of the shear wave velocity between sensors A4 to A5 and A3 to A5 resulted in reduction factors of R_S=0.85 and R_S=0.6, respectively. A graphical presentation of the shear wave velocity reduction in the proximity of the pile is presented in Fig. 13, along with an elevation view of the buried accelerometer locations at M-139 site. It should be noted that the degradation of the shear wave velocity will be higher at the pile-soil interface, i.e. the plastic zone very close to the pile. The quantification of the shear wave velocity in the non-linear zone close to the pile supports the hypothesis of different soil behavior zones around a driven pile, as presented in Fig. 12.

CONCLUSIONS

Ground vibrations were measured during driving of H-piles with diesel hammers at 5 sites around Michigan and some results from one of the sites are presented here. Ground motions were recorded by installing sensors in the ground, starting as close as 0.2 m from the pile, to capture the complex energy transfer mechanisms as the pile penetrates deeper into the ground during driving. A surface array of sensors that is traditionally used was also implemented. Analysis of the recorded data show that there are two types of waves that reach the buried sensors. When the pile tip is still above the sensor, spherical waves from the tip will impact the sensor. As the pile tip passes below the sensor elevation, cylindrical waves from the shaft will start to contribute. Surface ground motions revealed that the surface waves are not the classical Rayleigh wave forms that researchers have usually assumed. It is traditionally assumed that the surface waves propagating from an impact driven pile are Rayleigh waves and consequently, the vertical component of motion is only measured. However, in this study the horizontal components of motion were both or either greater

than the vertical amplitudes. This observation was found for other tested sites as well, and will be reported in a future publication.

The Fourier spectra of the three components of ground motion recorded by the three embedded sensors provided a range of frequencies from 0 to 100 Hz. High frequencies recorded by the vertical components of the sensors seem to diminish as the waves travel farther away from the pile. However, this trend was not observed for the two horizontal component amplitudes, where the frequency content was distributed over a wider band even when the waves have travelled farther away from the source.

Shear wave velocity degradation in the near field of an impact driven pile was evaluated by studying shear wave arrival times at sensors located in the ground at three distances from the pile. It was found that around 0.5 m from the pile, the shear wave velocity is about 0.4 times of the small strain shear wave velocity measured in the far field. It is anticipated that the shear wave velocity drops even more at the pile-soil interface, where the soil is sheared with high strains. This quantification of the shear wave velocity reduction in the non-linear zone very close to the pile, was not proven with physical ground motions until now.

ACKNOWLEDGMENTS

This work was funded by the Michigan Department of Transportation, project #114128, contract 2010-0296.

REFERENCES

[1] Heckman, W. S. and Hagerty, D. J., "Vibrations Associated with Pile Driving", *Journal of the Construction Division*, ASCE, Vol. 104, No. CO4, 1978, pp. 385-394.

[2] Clough, G. W., and Chameau, J-L., "Measured effects of vibratory sheetpile driving", *Journal of the Geotechnical Engineering Division*, ASCE, Vol. 106, GT10, 1980, pp. 1081-1099.

[3] Woods, R. D., and Jedele, L. P., "Energy-Attenuation Relationships from Construction Vibrations", Vibration problems in geotechnical engineering, ASCE, *Proceedings of a symposium sponsored by the Geotechnical Engineering Division*, Detroit, Michigan, October 22, 1985, pp. 229-246.

[4] Selby, A. R., "Ground vibrations caused by pile installation", *Fourth International Conference on Piling and Deep Foundations*, Stresa, Italy, April 7-12, 1991, DFI, pp. 497-502.

[5] Attewell, P. B., Selby, A. R. and O'Donnell, L., "Estimation of ground vibration from driven piling based on statistical analyses of recorded data", *Geotechnical and Geological Engineering*, Vol. 10, No. 1, 1992, pp. 41-59, doi: 10.1007/BF00881970.

[6] Linehan, P. W., Longinow, A. and Dowding, C. H., "Pipe response to pile driving and adjacent excavation", *Journal of Geotechnical Engineering*, ASCE, Vol. 118, No. 2, 1992, pp.300-316, doi: 10.1061/(ASCE)0733-9410(1992)118:2(300).

[7] Lewis, M. R. and Davie, J. R., "Vibrations due to pile driving", *Third International Conference on Case Histories in Geotechnical Engineering*, St. Louis, Missouri, June 1-4, 1993, pp. 649-655.

[8] Hwang, J. H., Liang, N. and Chen, C. H., "Ground Response during Pile Driving", *Journal of Geotechnical and Geoenvironmental Engineering*, ASCE, Vol. 127, No. 11, 2001, pp. 939-949, doi: 10.1061/(ASCE)1090-0241(2001)127:11(939).

[9] Kim, D. S. and Lee, J. S., "Propagation and attenuation characteristics of various ground vibrations", *Soil Dynamics and Earthquake Engineering*, Vol. 19, No. 2, 2001, pp. 115-126, doi: 10.1016/S0267-7261(00)00002-6.

[10] Thandavamoorthy, T. S., "Piling in fine and medium sand-a case study of ground and pile vibration", *Soil Dynamics and Earthquake Engineering*, Vol. 24, No. 4, 2004, pp. 295-304, doi: 10.1016/j.soildyn.2003.12.005.

[11] Massarsch, K. R. and Fellenius, B. H., "Ground vibrations induced by pile driving", *Sixth International Conference on Case Histories in Geotechnical Engineering*, Missouri University of Science and Technology, Arlington, VA, August 11-16, 2008, 38p.

[12] Park, C. B., Miller, R. D., and Xia, J., "Multichannel analysis of surface waves", *Geophysics*, Vol. 64, No. 3, 1999, pp 800-808.

[13] Okada, H., 2003, "The Microtremor Survey Method", *Geophysical Monograph Series*, No. 12, Society of Exploration Geophysicists, 135p.

[14] Grizi, A., Athanasopoulos-Zekkos, A. and Woods, R. D., "Ground Vibration Measurements near Impact Pile Driving", *Journal of Geotechnical and Geoenvironmental Engineering*, ASCE, Vol. 142, No. 8, 2016, doi: 10.1061/(ASCE)GT.1943-5606.0001499.

[15] Athanasopoulos-Zekkos, A., Woods, R. D. and Grizi, A., "Effect of pile-driving induced vibrations on nearby structures and other assets", Final Report to Michigan Department of Transportation, ORBP Number OR10-046, No. RC-1600, 2013, 146p.

[16] Gkrizi, A., “Characterization of Pile Driving Induced Ground Motions”, Ph.D. Thesis, University of Michigan, Ann Arbor, Michigan, 2017, 822p.

[17] Woods, R. D., “Dynamic Effects of Pile Installations on Adjacent Structures”, *Synthesis of Highway Practice NCHRP 253*, Transportation Research Board, Washington, D.C., 1997, 86p.

[18] Massarsch, K. R., “Dynamic Compaction of Granular Soils”, State-of-the art report, Lecture Series: A Look Back for the Future, University of Zejiang, China, 1999, pp. 181-223.

List of Figure Captions

FIG. 1 (a) Soil conditions, (b) SPT and Vs profile, and (c) Penetration resistance at M-139 site

FIG. 2 Perspective view of buried and surface sensors at M-139 site (from [14])

FIG. 3 Accelerations recorded at three distances from the pile versus pile tip penetration depth for (a) Vertical, (b) Longitudinal, and (c) Transverse direction

FIG. 4 Vertical acceleration versus diagonal distance from pile tip to sensor (a) A3, (b) A4, and (c) A5

FIG. 5 Peak particle velocities recorded by surface sensors versus pile tip penetration depth for (a) Vertical, (b) Longitudinal, and (c) Transverse direction

FIG. 6 Vertical component acceleration histories and frequency content of a single blow for (a) A3, (b) A4, and (c) A5 sensor with pile driving depth between 6.4 m to 6.7 m

FIG. 7 Longitudinal component acceleration histories and frequency content of a single blow for (a) A3, and (b) A5 sensor with pile driving depth between 6.4 m to 6.7 m

FIG. 8 Transverse component acceleration histories and frequency content of a single blow for (a) A3, (b) A4, and (c) A5 sensor with pile driving depth between 6.4 m to 6.7 m

FIG. 9 Vertical component acceleration histories and frequency content of a single blow for (a) A3, (b) A4, and (c) A5 sensor with pile driving depth between 8.8 m to 9.1 m

FIG. 10 Longitudinal component acceleration histories and frequency content of a single blow for (a) A3, and (b) A5 sensor with pile driving depth between 8.8 m to 9.1 m

FIG. 11 Transverse component acceleration histories and frequency content of a single blow for (a) A3, (b) A4, and (c) A5 sensor with pile driving depth between 8.8 m to 9.1 m

FIG. 12 Hypothetical soil behavior zones near a driven pile (modified after [18])

FIG. 13 Shear wave velocity degradation in the vicinity of a driven pile

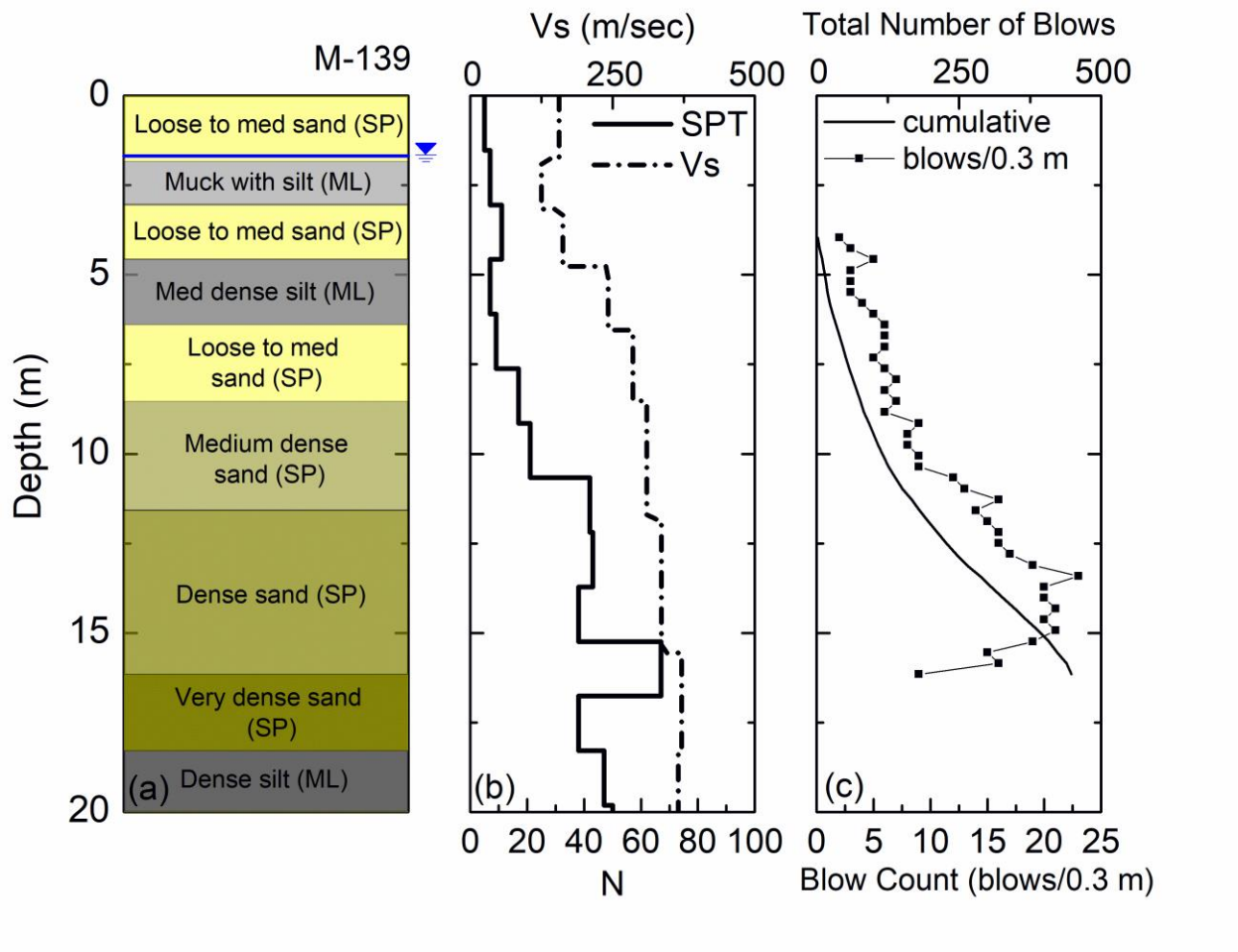
M-139
Loose to med sand (SP)
Muck with silt (ML)
Loose to med sand (SP)
Med dense silt (ML)
Loose to med sand (SP)
Medium dense sand (SP)
Dense sand (SP)
Very dense sand (SP)
Dense silt (ML)
(a)
Depth (m)
0
5
10
15
20
Vs (m/sec)
0
250
500
SPT
Vs
(b)
0 20 40 60 80 100
N
Total Number of Blows
0
250
500
cumulative
blows/0.3 m
(c)
0 5 10 15 20 25
Blow Count (blows/0.3 m)

Fig. 1

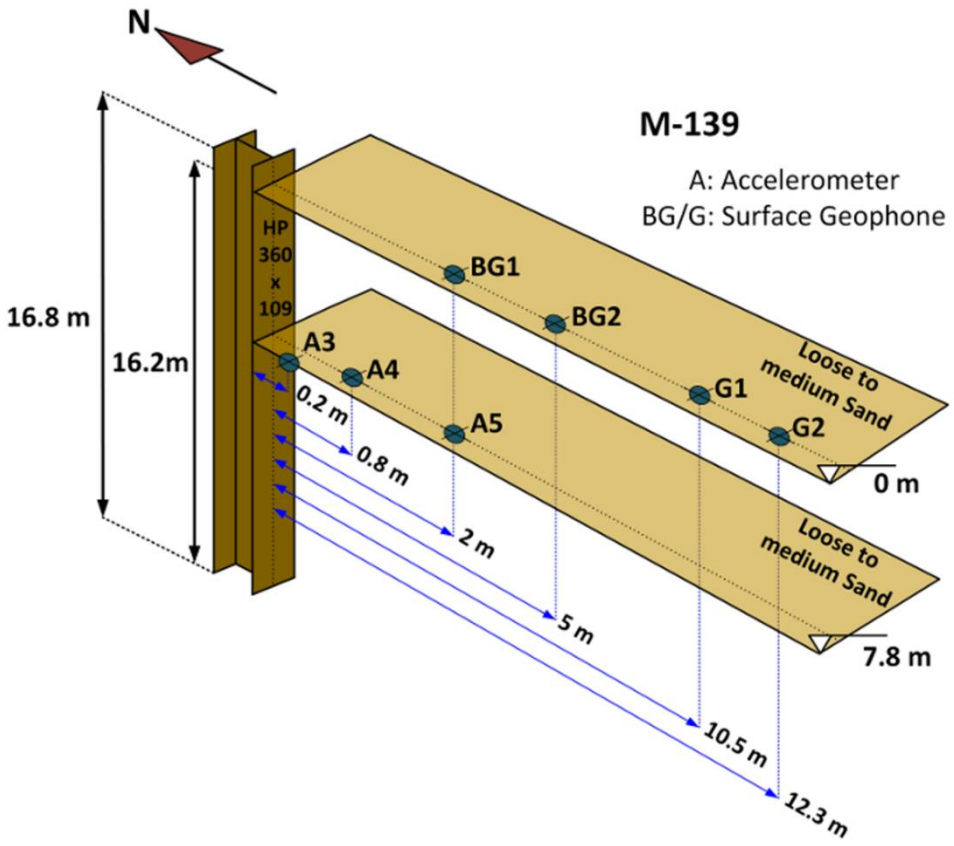
N
M-139
A: Accelerometer
BG/G: Surface Geophone
HP
360
x
109
16.8 m
16.2m
BG1
BG2
A3
A4
A5
G1
G2
Loose to
medium Sand
0 m
Loose to
medium Sand
7.8 m
0.2 m
0.8 m
2 m
5 m
10.5 m
12.3 m

Fig. 2

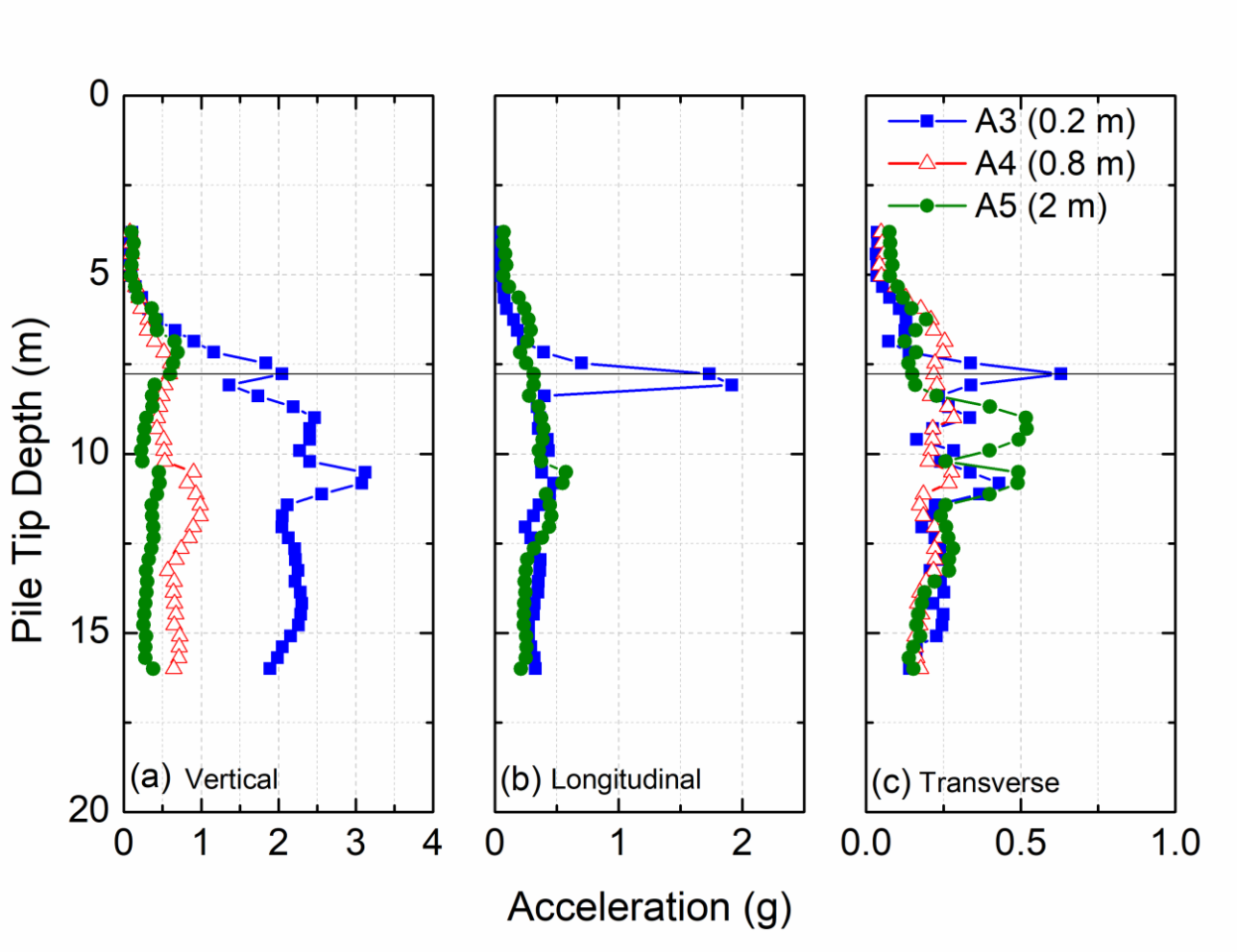
Pile Tip Depth (m)
0
5
10
15
20
(a) Vertical
(b) Longitudinal
(c) Transverse
A3 (0.2 m)
A4 (0.8 m)
A5 (2 m)
0
1
2
3
4
0.0
0.5
1.0
Acceleration (g)

Fig. 3

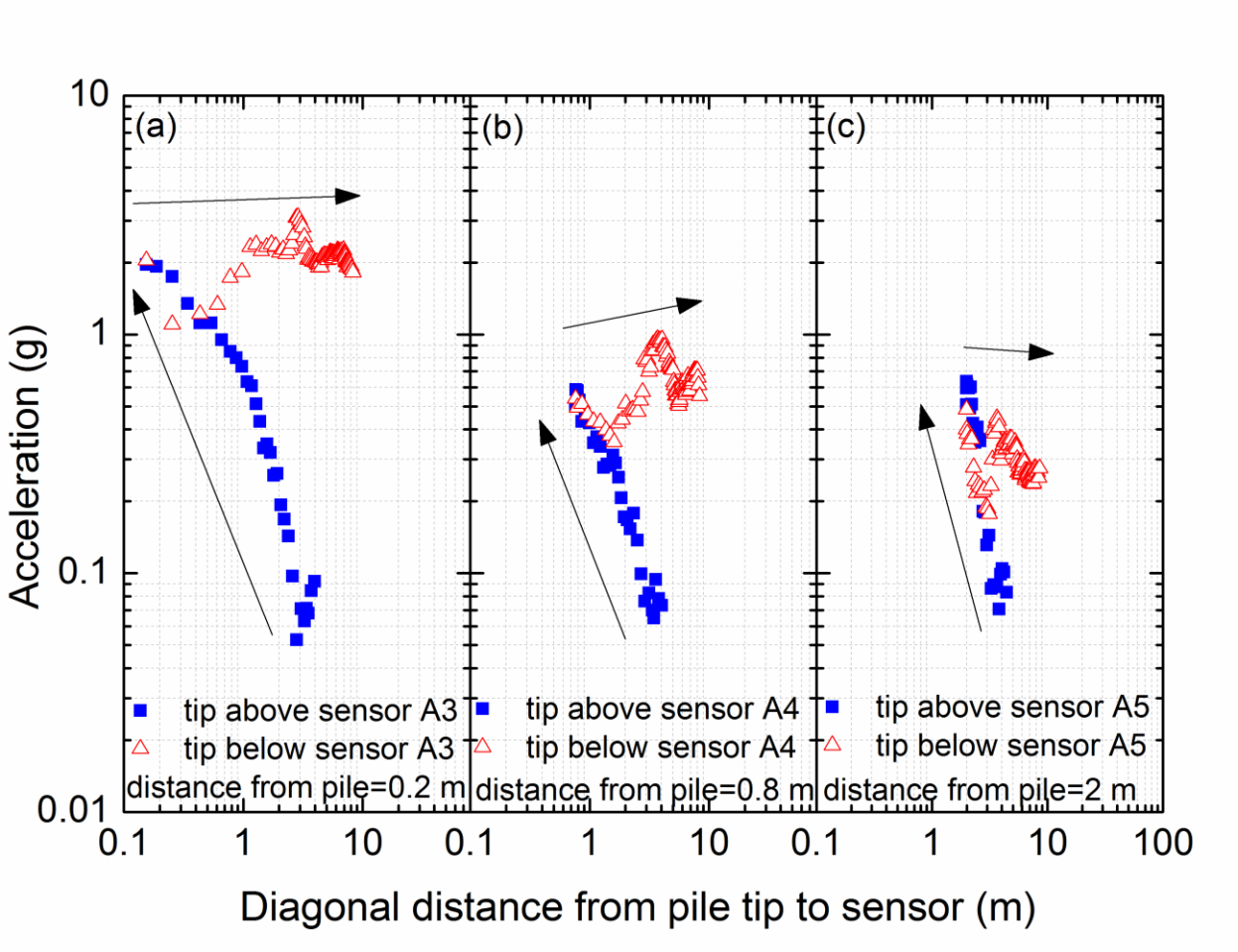
(a)
(b)
(c)
Acceleration (g)
10
1
0.1
0.01
tip above sensor A3
tip below sensor A3
distance from pile=0.2 m
tip above sensor A4
tip below sensor A4
distance from pile=0.8 m
tip above sensor A5
tip below sensor A5
distance from pile=2 m
0.1
1
10
100
Diagonal distance from pile tip to sensor (m)

Fig. 4

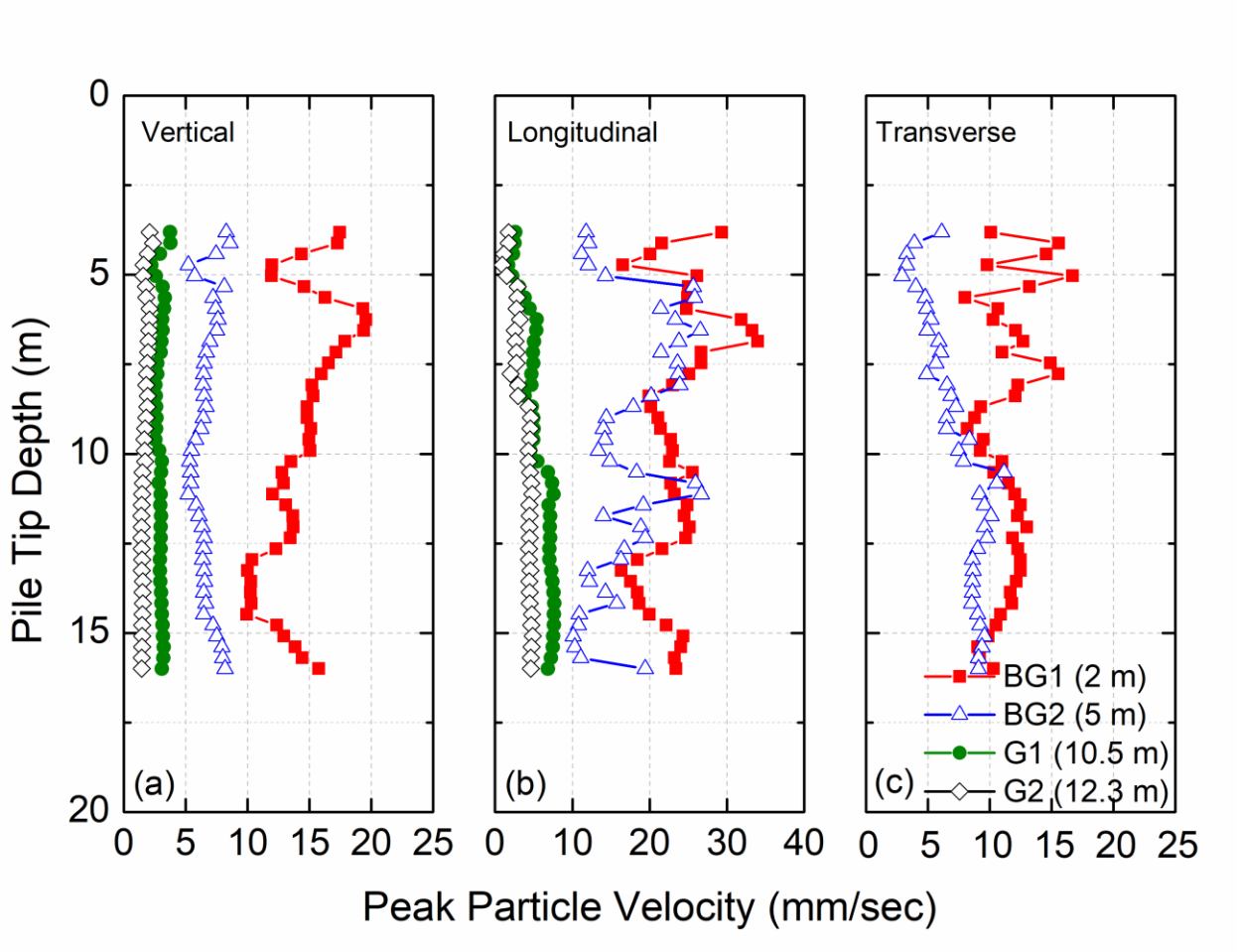
Vertical
Longitudinal
Transverse
(a)
(b)
(c)
Pile Tip Depth (m)
Peak Particle Velocity (mm/sec)
BG1 (2 m)
BG2 (5 m)
G1 (10.5 m)
G2 (12.3 m)
0
5
10
15
20
25
30
40

Fig. 5

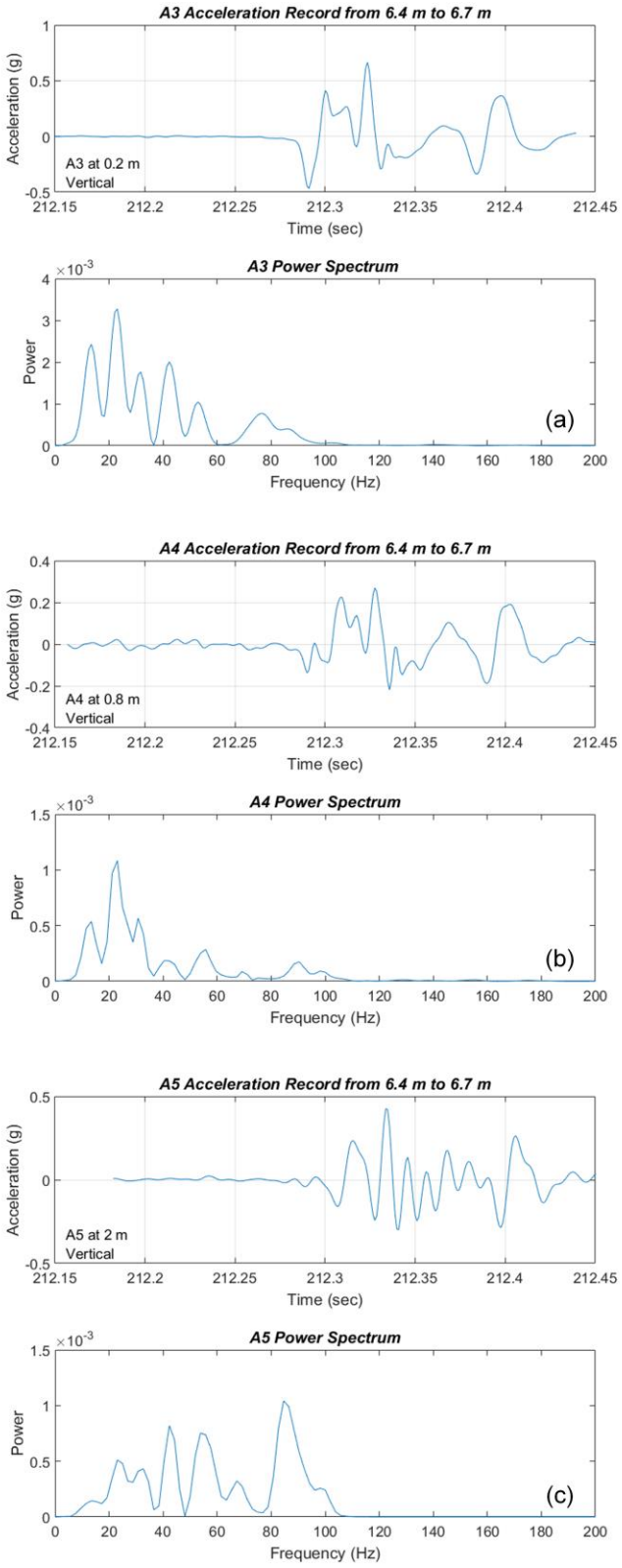
A3 Acceleration Record from 6.4 m to 6.7 m
Acceleration (g)
A3 at 0.2 m
Vertical
Time (sec)
A3 Power Spectrum
Power
(a)
Frequency (Hz)
A4 Acceleration Record from 6.4 m to 6.7 m
Acceleration (g)
A4 at 0.8 m
Vertical
Time (sec)
A4 Power Spectrum
Power
(b)
Frequency (Hz)
A5 Acceleration Record from 6.4 m to 6.7 m
Acceleration (g)
A5 at 2 m
Vertical
Time (sec)
A5 Power Spectrum
Power
(c)
Frequency (Hz)

Fig. 6

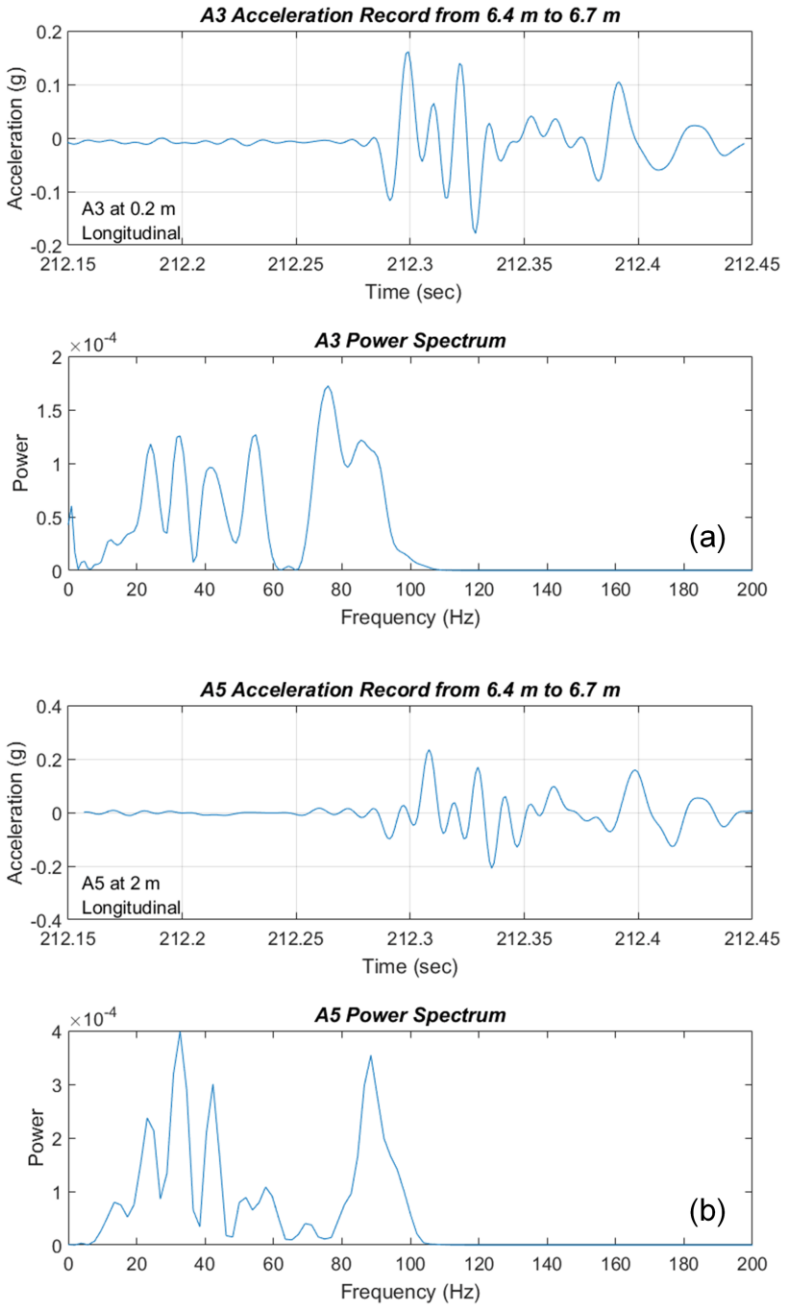
A3 Acceleration Record from 6.4 m to 6.7 m
Acceleration (g)
A3 at 0.2 m
Longitudinal
Time (sec)
A3 Power Spectrum
Power
(a)
Frequency (Hz)
A5 Acceleration Record from 6.4 m to 6.7 m
Acceleration (g)
A5 at 2 m
Longitudinal
Time (sec)
A5 Power Spectrum
Power
(b)
Frequency (Hz)

Fig. 7

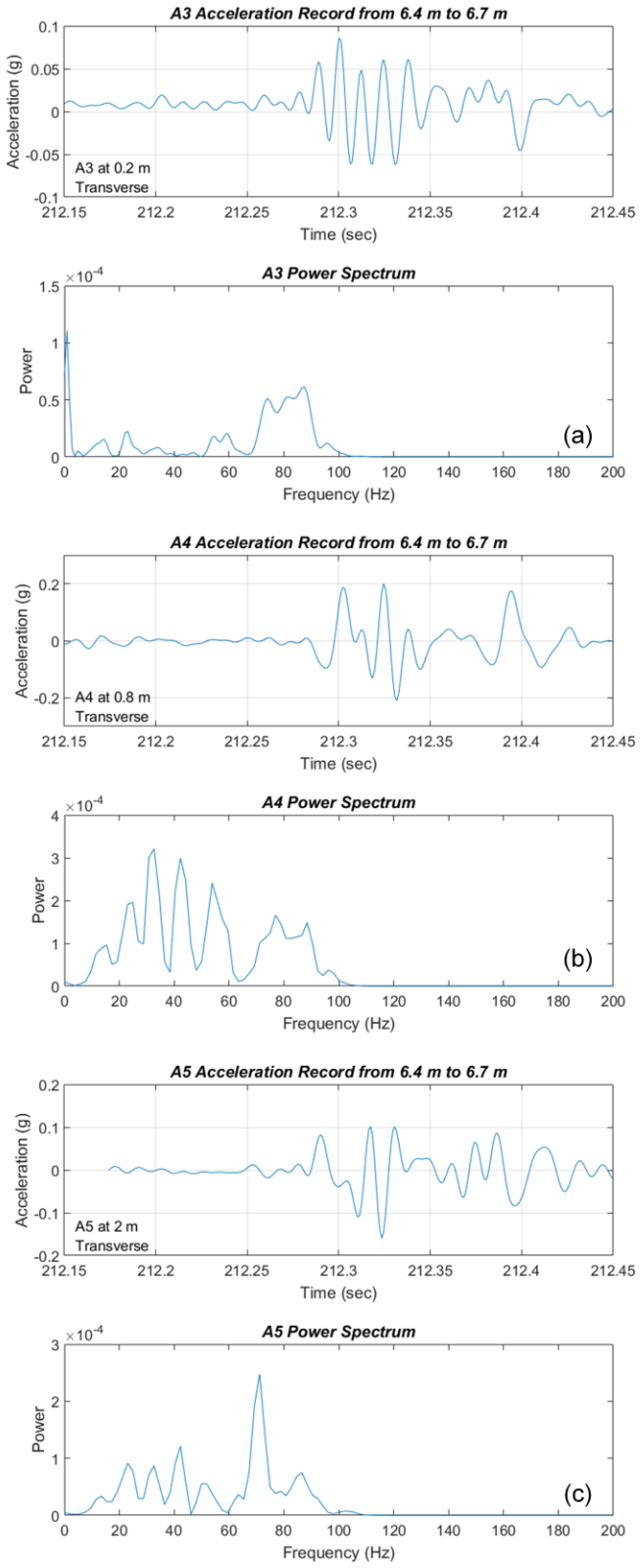
A3 Acceleration Record from 6.4 m to 6.7 m
Acceleration (g)
A3 at 0.2 m
Transverse
Time (sec)
A3 Power Spectrum
Power
(a)
Frequency (Hz)
A4 Acceleration Record from 6.4 m to 6.7 m
A4 at 0.8 m
Transverse
A4 Power Spectrum
(b)
A5 Acceleration Record from 6.4 m to 6.7 m
A5 at 2 m
Transverse
A5 Power Spectrum
(c)

Fig. 8

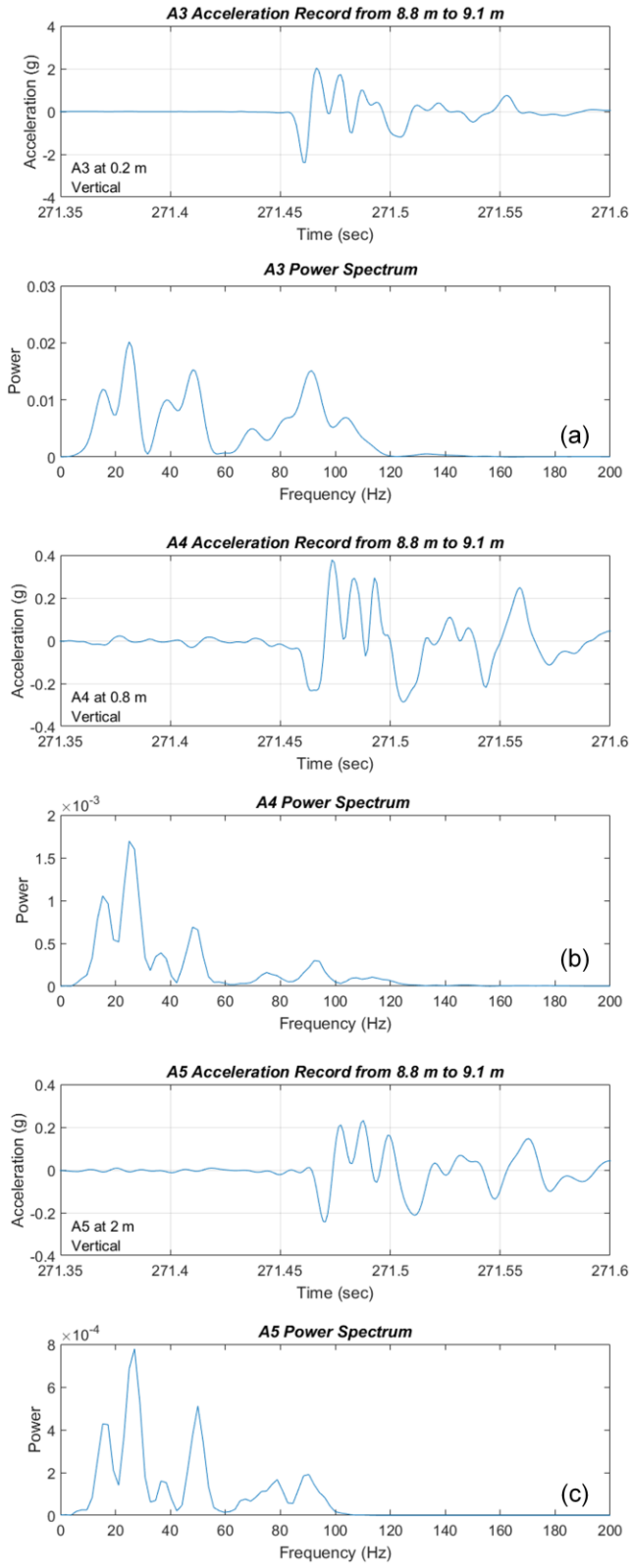
A3 Acceleration Record from 8.8 m to 9.1 m
Acceleration (g)
A3 at 0.2 m
Vertical
Time (sec)
A3 Power Spectrum
Power
(a)
Frequency (Hz)
A4 Acceleration Record from 8.8 m to 9.1 m
Acceleration (g)
A4 at 0.8 m
Vertical
Time (sec)
A4 Power Spectrum
×10-3
Power
(b)
Frequency (Hz)
A5 Acceleration Record from 8.8 m to 9.1 m
Acceleration (g)
A5 at 2 m
Vertical
Time (sec)
A5 Power Spectrum
×10-4
Power
(c)
Frequency (Hz)

Fig. 9

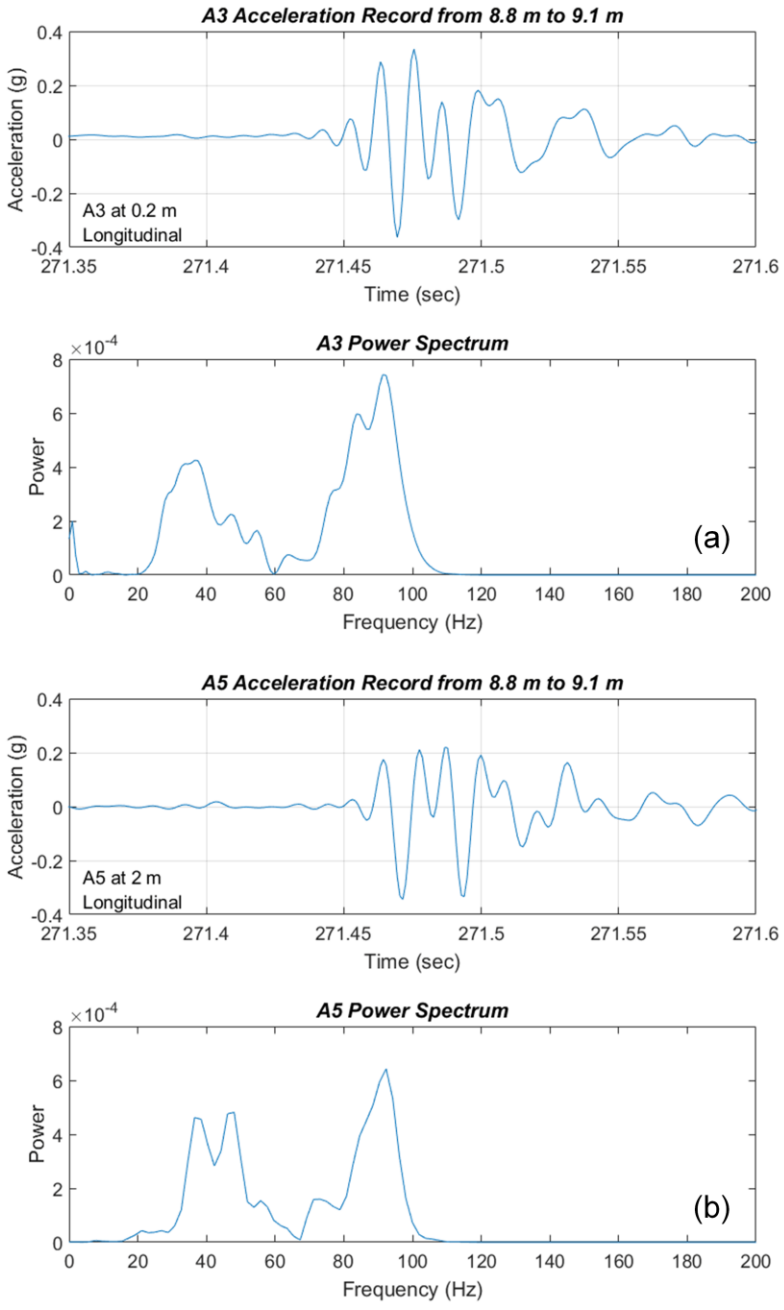
A3 Acceleration Record from 8.8 m to 9.1 m
Acceleration (g)
A3 at 0.2 m
Longitudinal
Time (sec)
A3 Power Spectrum
Power
(a)
Frequency (Hz)
A5 Acceleration Record from 8.8 m to 9.1 m
Acceleration (g)
A5 at 2 m
Longitudinal
Time (sec)
A5 Power Spectrum
Power
(b)
Frequency (Hz)

Fig. 10

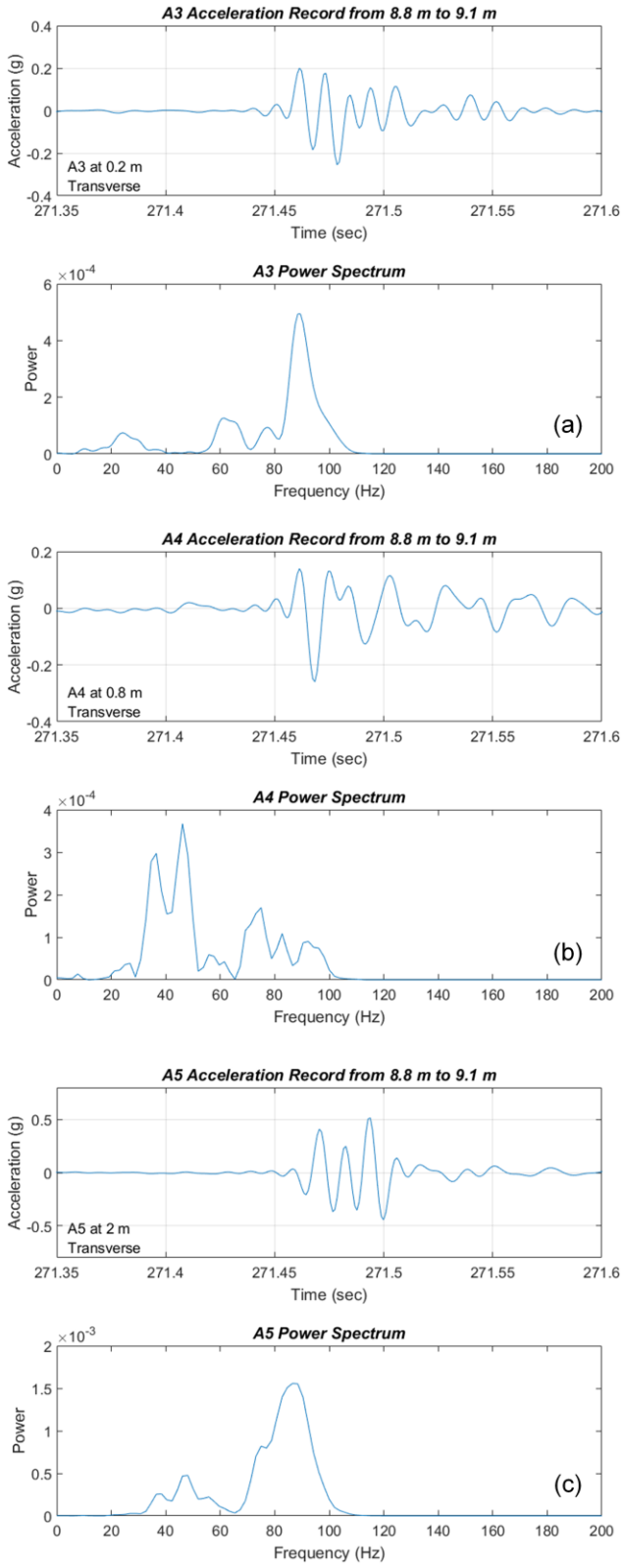
A3 Acceleration Record from 8.8 m to 9.1 m
Acceleration (g)
A3 at 0.2 m
Transverse
Time (sec)
A3 Power Spectrum
Power
(a)
Frequency (Hz)
A4 Acceleration Record from 8.8 m to 9.1 m
Acceleration (g)
A4 at 0.8 m
Transverse
Time (sec)
A4 Power Spectrum
Power
(b)
Frequency (Hz)
A5 Acceleration Record from 8.8 m to 9.1 m
Acceleration (g)
A5 at 2 m
Transverse
Time (sec)
A5 Power Spectrum
Power
(c)
Frequency (Hz)

Fig. 11

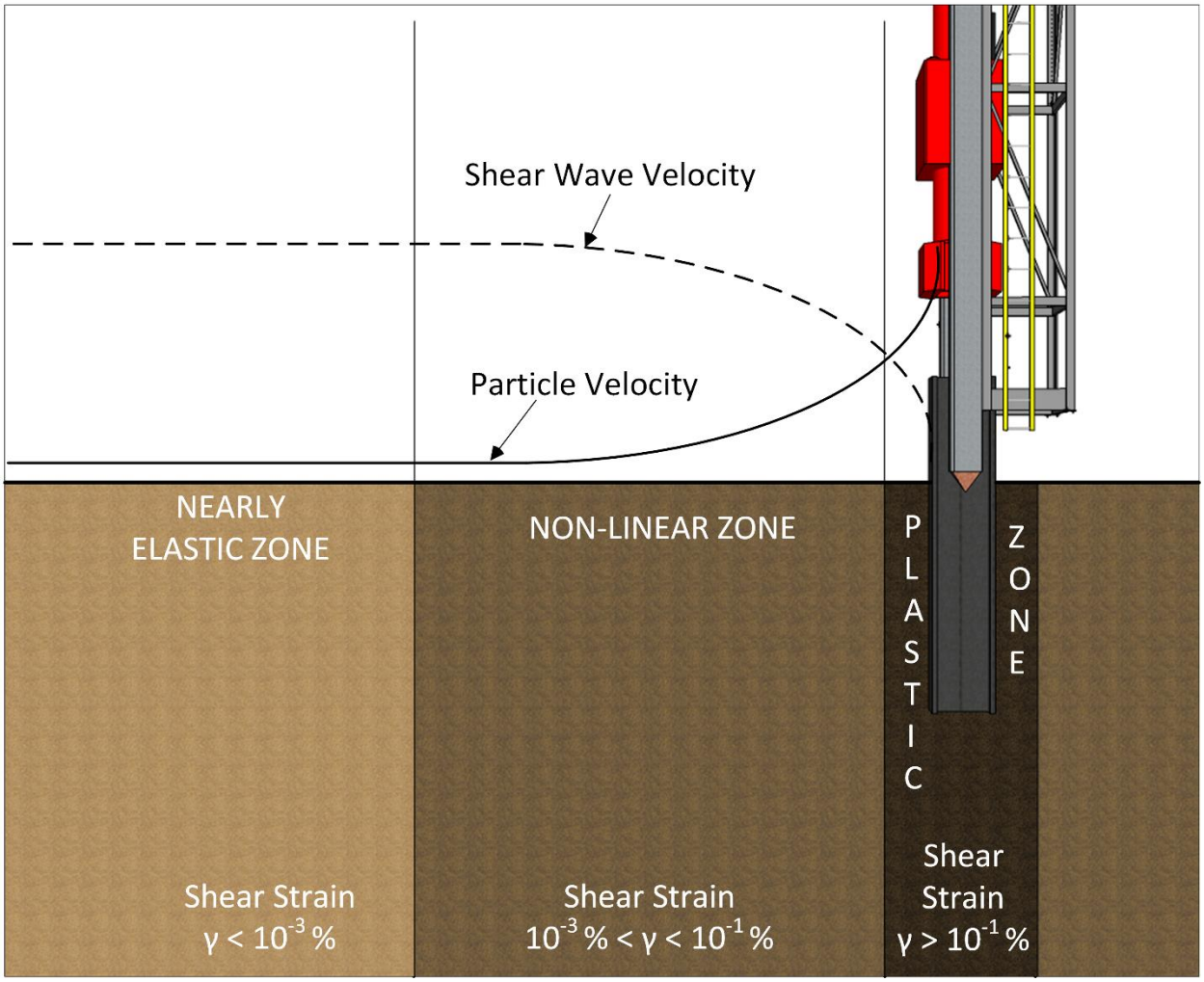
Shear Wave Velocity
Particle Velocity
NEARLY
ELASTIC ZONE
NON-LINEAR ZONE
PLASTIC ZONE
Shear Strain
γ < 10-3 %
Shear Strain
10-3 % < γ < 10-1 %
Shear Strain
γ > 10-1 %

Fig. 12

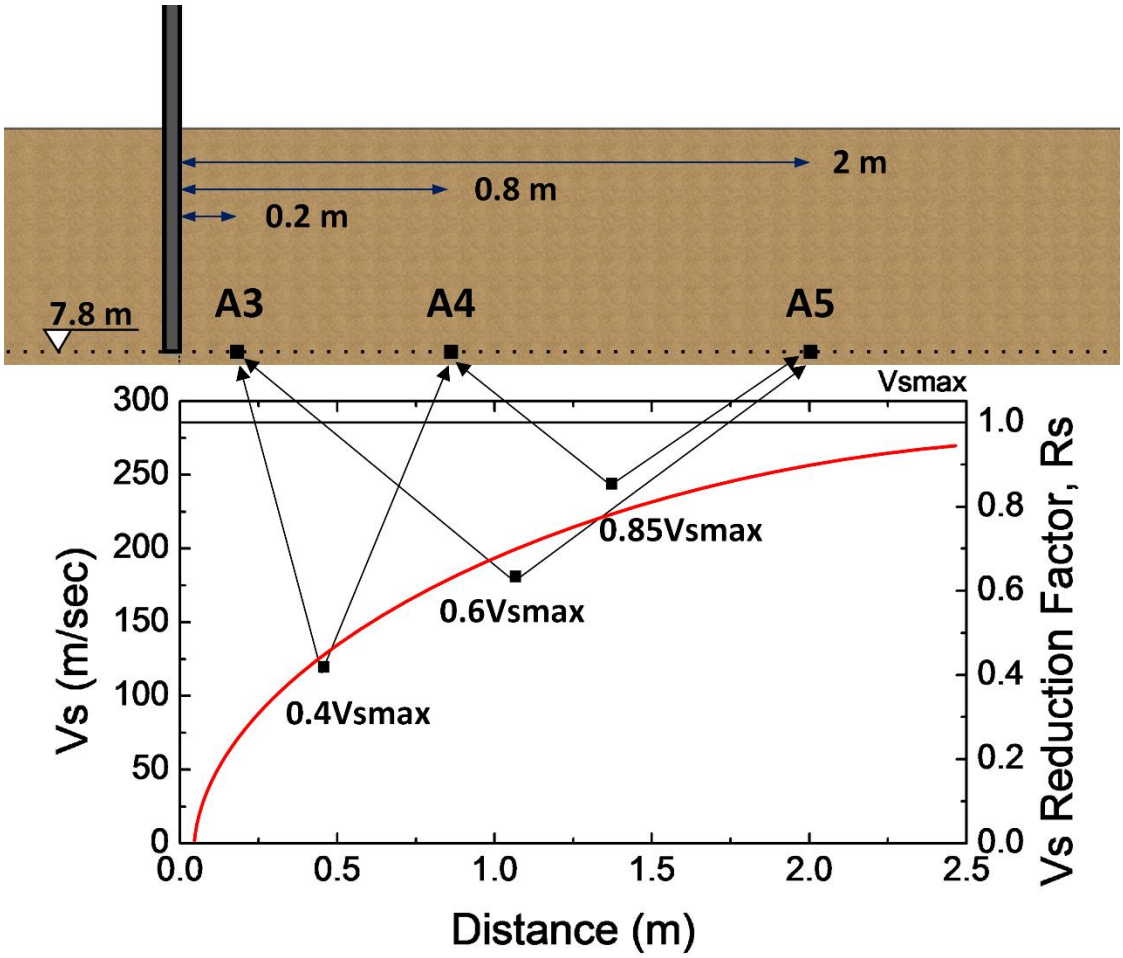
2 m
0.8 m
0.2 m
7.8 m
A3
A4
A5
Vsmax
0.85Vsmax
0.6Vsmax
0.4Vsmax
Vs (m/sec)
Vs Reduction Factor, Rs
Distance (m)
300
250
200
150
100
50
0
1.0
0.8
0.6
0.4
0.2
0.0
0.0
0.5
1.0
1.5
2.0
2.5

Fig. 13